Journal of Kufa for Chemical Sciences Vol. (4) No. (2) ………………….………….Jun. 2025

Article

Thermodynamic and Kinetic Study for adsorption of Congo Red Dye from Aqueous Solution over Magnetic Ferrite Nanoparticle

Atyaf M. Kadhem[1*] and Tariq Z. Jassim[1]

[1]Department of Chemistry, College of Education for Pure Sciences, University of Basrah, Basrah, Iraq

***Corresponding author email: atyafmd04@gmail.com**

Abstract

The synthesis of ferrite nanoparticles (NPs) with a $CuFe_20_4$ structure was accomplished via the auto-combustion method of sol-gel. Characterization of the nanomaterials was conducted utilizing Field emission-scanning electron microscopy (FE-SEM), fourier-transform infrared spectroscopy (FTIR), and X-ray diffraction (XRD) procedures. Investigation into the impact of contact duration, temperature, and pH on the CR dye's adsorption characteristics was undertaken. Optimal equilibrium was observed to be attained at a contact duration of 360 minutes within a pH range spanning from 3 to 11. A comparison between the Freundlich and Langmuir models showed a clear inclination of the adsorption data towards the Langmuir model. Thermodynamic assessment revealed a spontaneous nature of the process, with ΔG indicating spontaneity, ΔH denoting exothermicity, and ΔS exhibiting negative values indicative of reduced disorderliness and unpredictability in the adsorption phenomenon.

Keywords: Adsorption, CR dye, Ferrite nano particles, Langmuir and Freundlich model, thermodynamic and kinetic.

Introduction

The introduction of unacceptable foreign materials into the environment because of significant manufacturing expansion and modernization is known as pollution [1], One of the most crucial components that are utilized extensively in numerous sectors, including the textile one, is synthetic dye [2]. There are currently over 10,000 commercially available dyes [3], According to calculations, during the dying process, 10–25% the colors are eliminated from the effluent [4]. The solubility of dissolved oxygen, water transparency, sunlight permeability, and aquatic life are all negatively impacted by water with extremely small levels of dye (certain dyes at less than 1 ppm). This can also have an impact on the food chain [5]. Because certain colors are poisonous and carcinogenic, dumping them into waste water without first undergoing sophisticated treatment harms the environment and the ecology [6]. Consequently, getting rid of them became essential. Aqueous solution dye release has been evaluated employing a variety of techniques, for example wagulation, adsorption, ion exchange, chemical precipitation, and sedimentation [7-9].

The most successful method that has been used to remove dye from waste water appears to be adsorption [10]. Recently, it was discovered that spinel ferrites are a new family of adsorbents that work well for treating water [11, 12] Its huge surface area and numerous efficient spots make it appropriate for the removal of contaminants. Because of their super paramagnetic characteristics (SPM), using an magnetic field outside the body, the reaction mixture able to readily distinct from spinel ferrites [13, 14]. The spinel ferrites' capacity to extract nutritional salts, hazardous metals, and organic molecules from wastewater has been investigated [15]. These compounds are manufactured using various processes and techniques as either powders or thin films. One of the most widely used techniques is the sol-gel approach [16, 17], precipitation technique [18], hydrothermal method [19] and the auto-combustion sol-gel method [20]. Using locally available citric acid as fuel and surfactant, the technique of sol-gel auto-combustion was applied. in the current work CuFe204 to manufacture the ferrite sample. This technology is thought to be more economical and ecologically friendly than conventional technology synthesis.

The aim of this work is to find for a surface that is with high degree of portability for CR dye adsorption, be used in the process of contamination of the aqueous solution in nature.

Materials and Methods

Synthesis of $CuFe_20_4$ nanoparticles

The following procedures were followed in order to synthesize $CuFe_20_4$: 4.3488 g of $Cu(NO_3)_2.3H_2O$ (M.W 241) and 14.54 g of $Fe(NO_3)_2.9H_2O$ (M.W 404) were combined and dissolved in 25 ml of 2 M citric acid solution. To maintain the pH of the mixture at 7.0 while continuously swirling it with a magnetic stirrer, ammonia solution (NH_4OH) was added. After 30 minutes of constant stirring at 80°C, the clear solution fully gelled. To get a consistent weight, desiccate in an oven at 80 °C. Grind to a finely ground powder. Calcined for three hours at 600 °C in an air-filled furnace.

Characterization

Numerous cutting-edge, extremely effective technologies that are employed globally have been used for diagnostics. energy dispersive X-ray spectroscopy (FESEM - EDX), Fourier Transform Infrared (FTIR), and X-ray diffraction (XRD)are utilized to depict these.

Adsorption Studies

The solution of congo red dye stock was made via dissolution 0.1 grams of dye in 100 milliliters of deionized water. In order to find the appropriate pH, several other diluted solutions were made from this concentration, and buffer was employed to maintain the pH range between 3 and 11. Using the batch approach, which involved adding 0.2 gm of the adsorbent to 50 milliliters dye solution at a 50 mg/L concentration and placing the mixture in a 100 ml flask, perfect contact was measured in 5 to 600 minutes. For various temperatures of 10, 20, 30, equilibration, and 50°C were utilized, together with a shaker in orbit set to agitate at a rate of 120 rpm.

After centrifuging the mixture, a spectrophotometer with UV-vis (UV-1200 spectrophotometer) was utilized to measure the dye's concentration. Equations were used to compute the equilibrium uptake of CR dye and its elimination efficiency.

$$\% \text{ Removal} = (C_o-C_e)/C_o * 100 \qquad (1)$$

$$Q_e = V(C_o-C_e)/m \qquad (2)$$

Where the equilibrium concentration is indicated by C_e (mg/L), V indicates the solution volume in liters, the dye concentration before to adsorption is represented by C_o (mg/L), and Q_e indicates the capacity of equilibrium adsorption (mg/g), m(g) indicates the adsorbent weight. The data on adsorption was analyzed using Langmuir and Freundlich isotherms.

Thermodynamic parameters

0.2 g of $CuFe_2O_4$ was added to each concentration after different concentrations, between 5 to 50 mg/L, were generated from the CR dye stock solution and put in flasks. After a 120-rpm shake was applied to the flasks. for the duration of the balance period at various temperatures of 10, 20, 30, and 50 °C, the CR dye concentration was ascertained after centrifuging the mixture. Equations (3-5) were utilized to calculate ΔG, which represents the fluctuations in enthalpy ΔH, free energy, and A entropy ΔS associated with the procedure of adsorption [21].

$$\Delta G=-RT \ln k \qquad (3)$$

$$K = C_{solid} / C_{liquid} \qquad (4)$$

$$\ln k = \Delta S/R - \Delta H/RT \qquad (5)$$

Equation (5) was used to calculate the slope and intersection quantities for ΔH (KJ.mol^{-1}) and ΔS (KJ.mol^{-1}. K^{-1}) based on the given parameters: The constant gas is denoted by R. (0.0083 KJ.K^{-1}. mol^{-1}), K represents the equilibrium constant, T denotes the temperature in Kelvin, the liquid phase's concentration at equilibrium (mg/L) is represented by C_{liquid}, and the solid phase's concentration at equilibrium (mg/L) is represented by C_{solid}. [22].

Kinetic study

The CR dye kinetic experiment on $CuFe_2O_4$ was conducted using 0.2 gm of nanoparticles that were placed in a 100 ml screw-capped conical flask. Using a water-bath temperature control system, A 120 rpm shake was applied to a variety samples. for 10, 20, 30, and 50 °C, including 50 milliliters of the tested dye at 50 mg/L concentration. The mixture solution was then removed at various times for measurement. The amount of dye adsorbed, as determined by Eq. (2), using spectrophotometry at 496 nm.

Results and Discussion

FT-IR specrum for the synthesized materials

FTIR spectrum for the synthesized materials at 600 °C are shown in Figure 1. This spectrum was recorded in range of 400 cm^{-1} to 4000 cm^{-1} and it showed several absorption peaks. The extending to the hydroxide (OH) bond's vibration, which shows the water's adsorption on ferrite, may be the cause of the peak 3415 cm^{-1} [23]. Spinel ferrite is situated between 400 and 600 cm^{-1} where (Fe–O) and (Cu–O) are stretching vibrations [24].

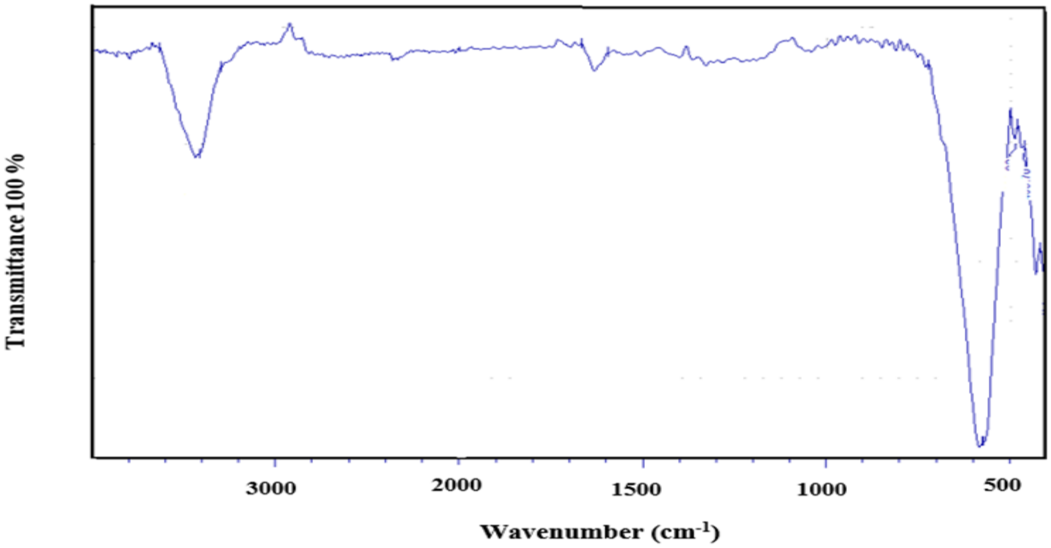

Fig. 1: FT-IR spectrum for the synthesized $CuFe_2O_4$

X-rays Diffraction (XRD)

XRD patterns for the synthesized materials are shown in figure 2, the sample heated to 600 °C was structurally analyzed. Size-controlled $CuFe_2O_4$ phase analysis is contrasted with (JCPDS No. 34-0425). which demonstrate that there is good agreement between the principal diffraction peaks at 2ϴ values, which are correspond to the pure structure miller planes (111), (220), (311), (222), (400), (420), (511), and (440). The Debye-Scherrer formula was applied in order to determine the crystal sizes for the X-ray spectra, and the results of the XRD analysis acquired during the current inquiry were discovered to be consistent with the reported results.

$$\tau\ hki = k*h/Bhki*\cos(\theta nki) \qquad (6)$$

In this case, θhki represents the Bragg angle of the (hki) peak, Bhki denotes the full width at half maximum, λ represents the wavelength of the x-ray, K denotes a constant equal to 0–9, and τ denotes the size of the particles with relation to the natural line of the (h K_1) plane [25]. The calculated particle size of $CuFe_2O_4$ nanoparticles is approximately 29.26 nanometers.

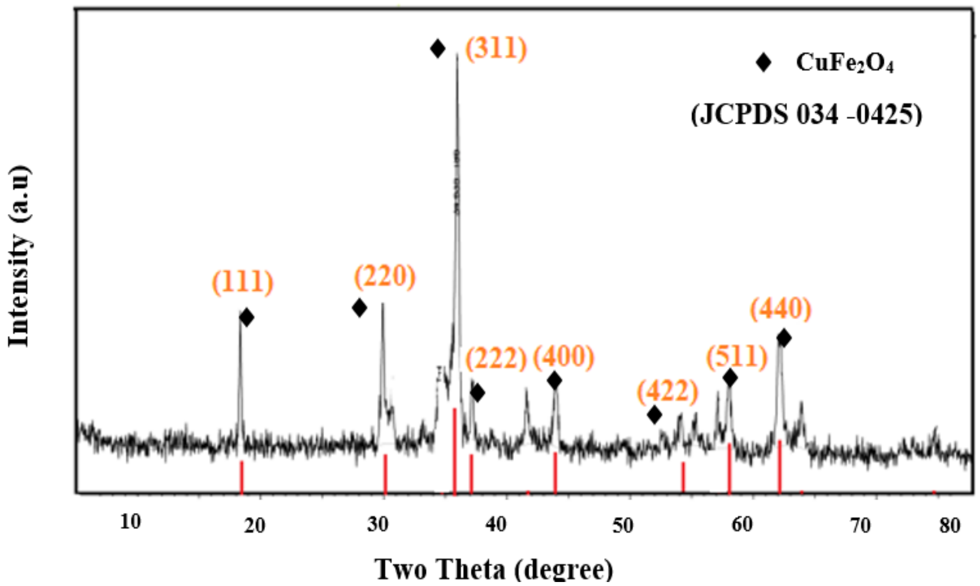

Fig. 2: XRD patterns for the synthesized $CuFe_2O_4$

Surface morphology and elemental analysis

An important tool in this process is the surface morphology analysis known as field emission scanning electron microscopy (FESEM). As the electron beam interacts with the sample surface during scanning, it creates a distinct pattern from which the surface attributes are derived. The particles were seen to be tightly packed, irregularly shaped agglomerates in the $CuFe_2O_4$ FESEM micrographs.

Collectively, one or more of the following processes may take place during the formation of $CuFe_2O_4$ particles. These are nucleation and growth surface-free energy required for the synthesis of $CuFe_2O_4$ is decreased. In addition to that, the element crystals aggregate due to the molecular attraction of distinct scale forces. The surface-free energy decreases as a result.

Aggregation is caused by the creation of new crystals inside the aggregates, which takes place while residual supersaturation is continuous. Subsequently, the agglomerated particles combine with more particles to form secondary particles, which grow larger. This agglomerated particle aggregates to produce an increase in particle size. Cu was found in the samples, as indicated by the EDX results, which also supported the appropriateness of the preparation process for $CuFe_2O_4$. FTIR, EDX, and $CuFe_2O_4$ with a pure crystal structure were also confirmed. Cu, Fe, and O pictures from the EDX are displayed in figure (3) [26].

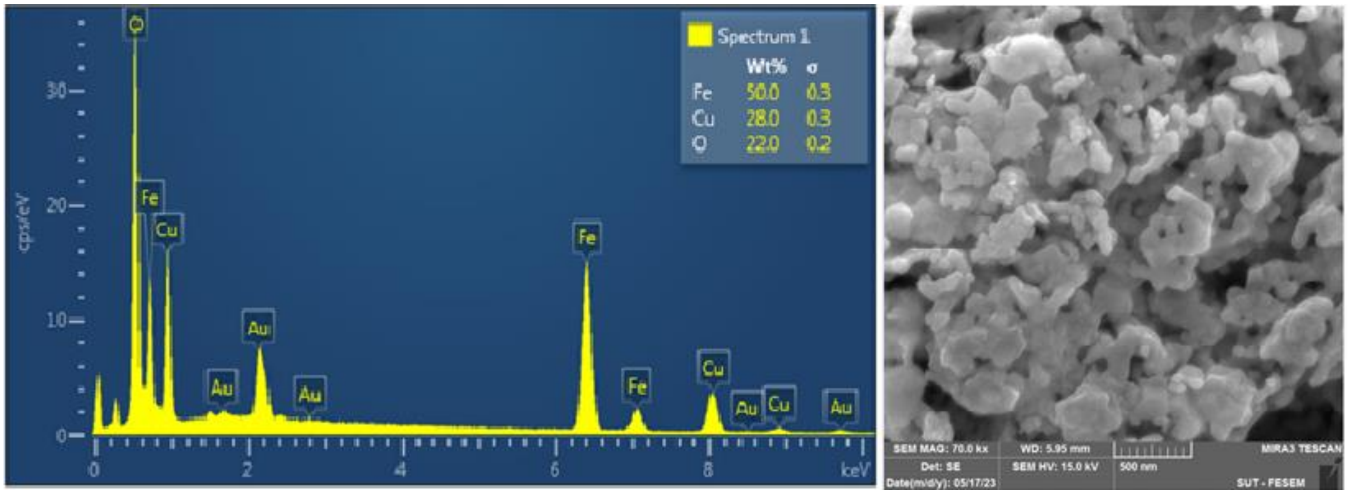

Fig. 3: FESEM micrographs and EDX af $CuFe_2O_4$ annealed at 600 °C

Adsorption studies

Contact time effect

The contact duration impact on the CR dye adsorption was examined throughout a range of times (5-600 min) at 25 °C constant temperature. Figure (4) illustrates how extending the duration of contact until equilibrium results in a rise in the exclusion percentage of CR dye. Due to the ample surface area, there is a significant potential for attaching the CR dye, there is a high adsorption amount at first. However, as equilibrium is established and the active sites are likely saturated, the adsorption rate slows down towards the end [27, 28]. The equilibrium time was 360 minutes, and 77.830% of the dye was found to have been removed.

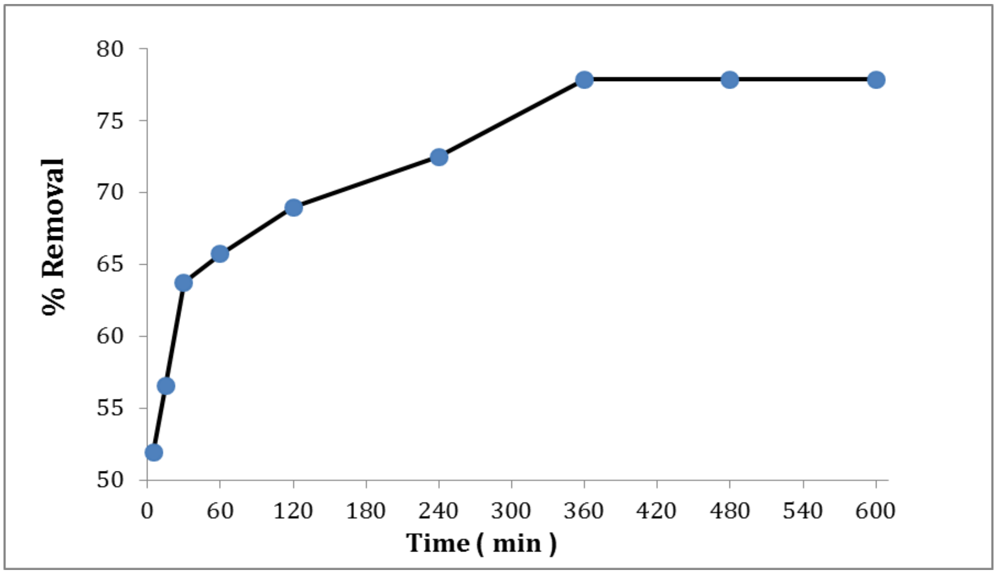

Fig. 4: The effect of contact time on adsorption of CR dye over $CuFe_2O_4$

pH's impact on the adsorption

One of the key elements influencing the dye adsorption onto an adsorbent is pH. Using a contact duration of 360 min, an applied concentration 50 mg/L, and an amount of nanoparticle adsorbent 0.2 gm at 25 °C, the effects of pH on the adsorption of CR dye on $CuFe_2O_4$ nanoparticle in various pH (3-11) were examined.

Figure 5 demonstrated how pH affected the adsorption process. The findings demonstrated that when pH accelerates between 3 and 11, the elimination percentage for CR decreases from 90.4% to 29.5% (see figure 5). $CuFe_2O_4$ positively charged surface and negatively charged anionic CR dye the exhibit a very high electrostatic attraction at pH=3, This phenomenon arises from the presence of acidity causing the active sites to become positively charged, characterized by low pH levels. The quantity of sites that are positively charged reduced as the system's pH risen, which in turn caused the base medium's adsorption capacity to decrease [29].

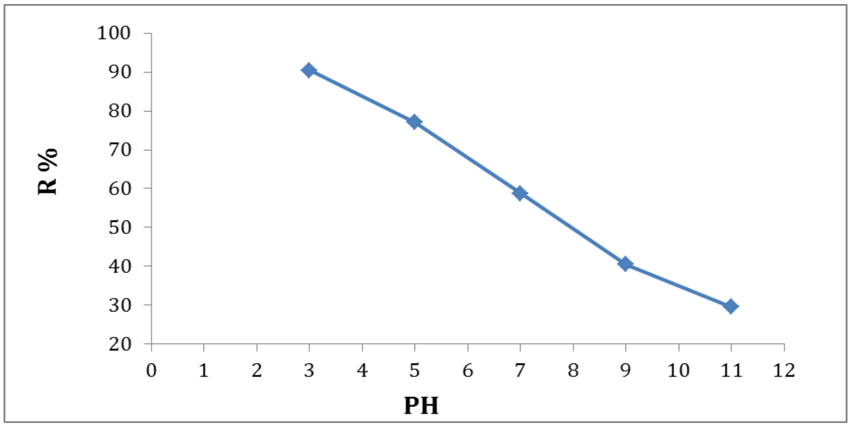

Fig. 5: pH effect on adsorption of CR dye over $CuFe_2O_4$

Adsorption isotherm

A range of temperatures, specifically 10, 20, 30, and 50 °C, were used to evaluate the ability of $CuFe_2O_4$ nanoparticles to extract CR dye from their aqueous solution. The quantities adsorbed onto CuFe2O4 nanoparticles (Q) are plotted against the equilibrium concentration (C_e) at temperatures of 10, 20, 30, and 50°C, illustrating the dye adsorption isotherm's fundamental form.

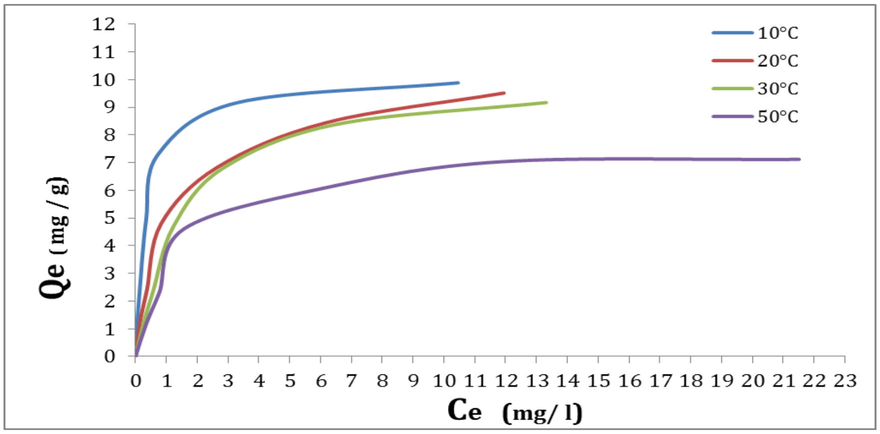

Fig. 6: Adsorption isotherm of dye on $CuFe_2O_4$ at various temperatures

The (S-type) Giles classification aligns with the shape of the CR dye adsorption isotherm on $CuFe_2O_4$. The vertical or plateau-like Adsorption alignment is reflected in the S-curve, indicating significant adsorption of the molten layer and strong intermolecular attraction within the adsorbent layer, resulting in the fixation of larger quantities [30]. Utilizing the Langmuir and Freundlich isotherm, the adsorption results were utilized. Then, applying Freundlich's Eq. (7) and Langmuir's Eq. (8), the impacts were investigated [31]. The data of isotherm adsorption are also included in Table (1).

$$\text{Log } Q_e = \log kf + 1/n \log C_e \tag{7}$$

where n denotes the adsorption intensity and Kf denotes a function of capacity for adsorption.

$$C_e/Q_e = 1/Q_m b + C_e/Q_m \tag{8}$$

where Q_m denotes the adsorption maximum capacity (mg/g) and b denotes a function of the sorption energy.

Plotting (C_e) vs (e/Q_e) and (log C_e) versus (log Q_e), respectively, on the experimental data of CR dye adsorption on CuFe2O4 allows the Freundlich and Langmuir isotherms to be used in Figures (7) and (8).

Table 1 shows that the Langmuir model's R^2 amounts for the adsorption process onto CuFe2O4 are closer to unity than the Freundlich model. This indicates that the Freundlich model was less successful than the Langmuir model. in characterizing the CR dye adsorption on $CuFe_2O_4$ nanoparticles. The findings indicate that the Langmuir isotherms are further appropriate than the Freundlich model for this system, as evidenced through (C_e/Q_e) and (Ce)'s linear relationship. displayed in figures (7, 8) [32].

Table 1: The outcomes obtained from employing the Freundlich and Langmuir isotherms on the investigated system.

	Temp. (°C)	Langmuir			Freundlich		
		Qm (mg/g)	b (g/mg)	R^2	Kf	n	R^2
CR dye	10	10.257	2.618	0.9998	5.494	2.565	0.8503
	20	10.332	0.859	0.9985	3.797	2.192	0.9292
	30	10. 459	0.573	0.9980	3.141	1.931	0.9115

	50	7.713	0.641	0.9981	2.511	2.386	0.8667

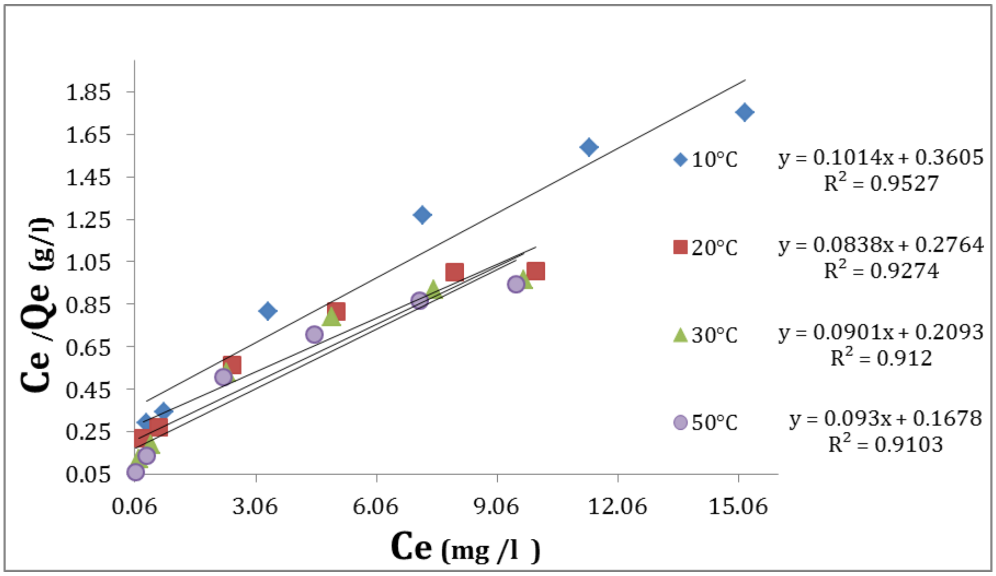

Fig. 7: Langmuir isotherm Linear form of CR dye on $CuFe_2O_4$ at various temperatures.

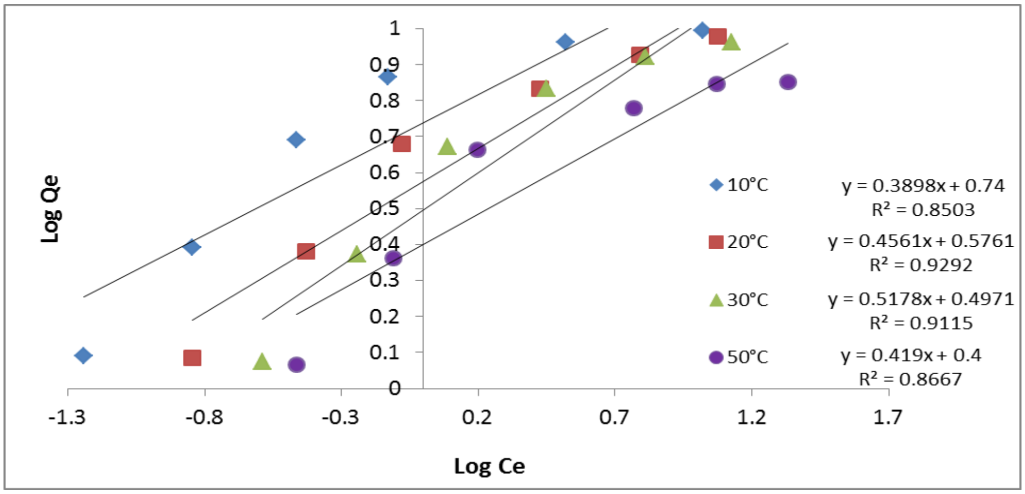

Fig. 8: Freundlich isotherm Linear form of CR dye on $CuFe_2O_4$ at various temperature

Thermodynamic Study

Temperature's effects on the adsorption of CR dye onto $CuFe_2O_4$ was assessed using equations involving parameters for example Gibbs energy change (ΔG), entropy change (ΔS), and enthalpy change (ΔH). These equations allowed the estimation of the adsorption process's effictiveness across temperatures ranging from 10 to 50 °C and varying initial concentrations [21].

$$\Delta G = - RT \ Lnk \tag{9}$$

$$K = C_{solid} / C_{liquid} \tag{10}$$

$$Lnk = \Delta S/R - \Delta H/RT \tag{11}$$

In the equation, K stands for the equilibrium constant, T stands for the temperature in Kelvin, R stands for the gas constant (0.0083 $KJ.K^{-1}.mol^{-1}$), C solid represents the equilibrium concentration in the solid phase (mg/L), and ΔS (KJ/mol.K) and ΔH (KJ/mol) can be approximated from the intercept and slope of Eq. (11) respectively. The thermodynamics parameters for the given ranges of temperature are listed in Table (2).

Table 2: Thermodynamic function for studied dye adsorption.

	Co (mg/L)	equilibrium constant (K)				- ΔG (KJ mol^{-1})				ΔH (KJ.mol^{-1})	ΔS (KJ.mol^{-1}. K^{-1})
		Temperature (°C)				Temperature (°C)					
		10	20	30	50	10	20	30	50		
CR dye	5	86.719	34.211	18.455	13.619	10.084	9.244	8.404	6.724	- 33.856	- 0.084
	10	69.422	25.954	16.513	11.970	9.376	8.596	7.816	6.256	- 31.450	- 0.078
	20	57.479	23.154	15.286	11.730	9.123	8.452	7.772	6.412	- 28.376	- 0.068
	30	39.431	10.290	9.608	4.097	8.063	6.973	5.883	3.703	- 38.910	- 0.109
	40	11.070	5.451	5.168	2.373	5.704	4.944	4.184	2.664	- 27.212	- 0.076
	50	3.781	3.186	2.755	1.324	3.515	2.935	2.355	1.195	- 19.929	- 0.058

With a correlation coefficient (R^2=0.8408-0.9464), it was discovered that the lnk against 1/T plots were linear. Adsorption on CuFe2O4 nanoparticles is shown in figure (9). It may be inferred from Table (2) that the adsorption process is spontaneous because ΔG was negative at every temperature [33]. Furthermore, the negative ΔH value suggests that the process of adsorption is exothermic, and the interface of solid solution is thought to have less disorder and randomness due to the negative value of ΔS [34].

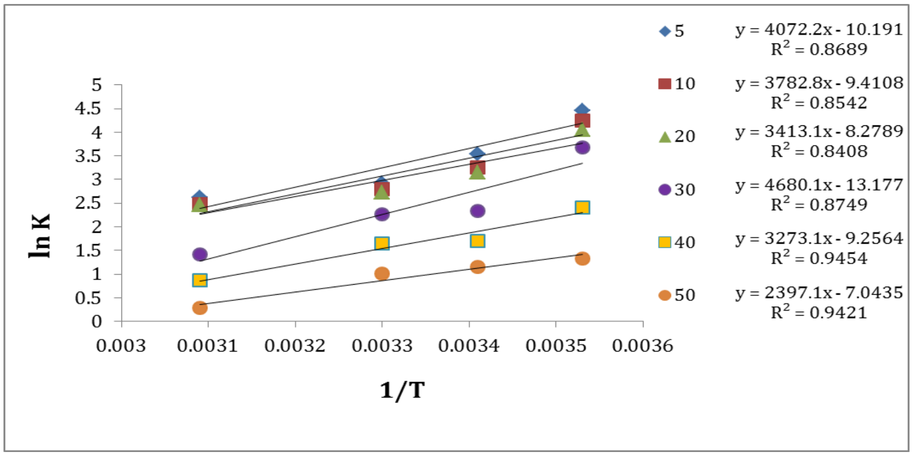

Fig. 9: Plot of lnk against 1/T for CR dye adsorption on $CuFe_2O_4$

Kinetics of adsorption

The adsorption kinetics data are analyzed utilizing the first-order pseudo (Lagergren equation) and pseudo-second-order (McKay and Ho) methods to elucidate the functional dynamics of the adsorption process. This is the pseudo-first-order rate equation:

$$\ln(Q_e - Q_t) = \ln Q_e - K_1 t \qquad (12)$$

(K_1) (hr^{-1}) denotes the first order adsorption rate constant, and the adsorbed dye on the CuFe2O4 nanoparticles quantities at equilibrium and time (t) in hours are denoted by (Qe) and (Qt) (mg/g), respectively. The results of applying the pseudo-first order rate Eq. (12), which finds the slope of (t) versus $\ln(Q_e\text{-}Q_t)$ given linear relationships, are displayed in Table (2) and figure (9). The calculated capacity value and K_1 are, respectively, estimated from the slope and intercept. The pseudo-second order average that is calculated is:

$$t/Q_t = 1/K_2 Q_e^2 + 1/Q_e (t) \qquad (13)$$

where the second order adsorption's rate constant is (K_2) $(g.mg^{-1}.hr^{-1})$. By using the pseudo-second order rate Equation (13), the plot of (t/Q_t) versus (t) provides linear relationships from which the slope and intercept are used to infer the calculated quantities of Q_e and K_2. The results obtained are displayed in Table (3) and figures (10, 11).

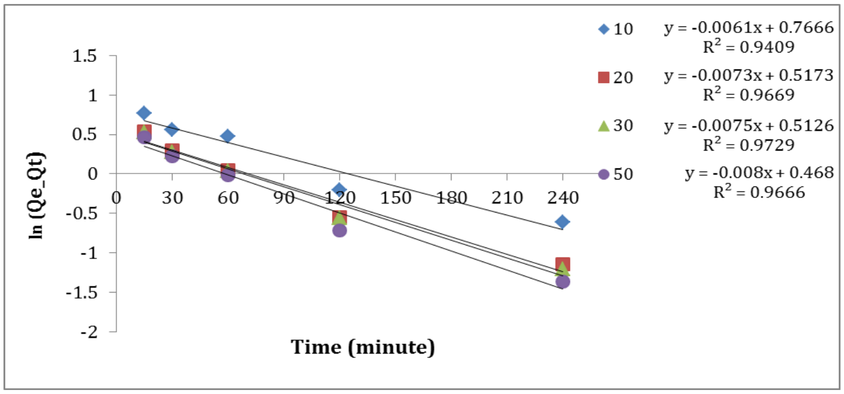

Fig. 10: pseudo-first order Kinetic model of CR dye on $CuFe_2O_4$ linear form at different temperature.

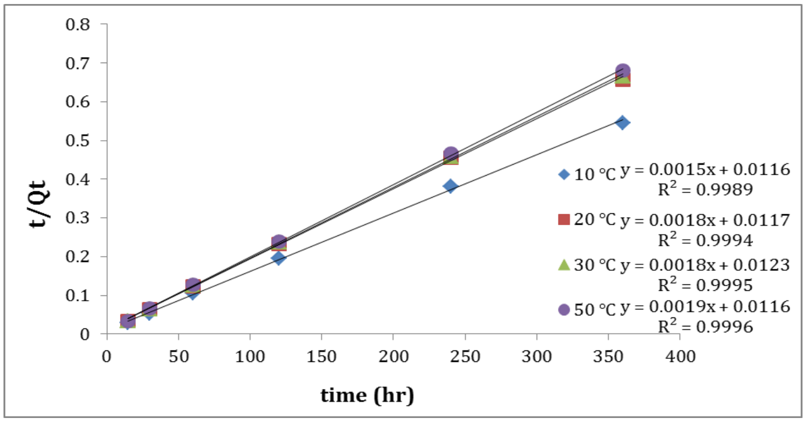

Fig. 11: pseudo-second order kinetic model of CR dye on $CuFe_2O_4$ linear form at different temperature.

Table 3: First order and second order kinetics rate constant calculated and experimental Q_e values and R^2.

CR Dye	Temp. (°C)	Pseudo-first order				Pseudo-second order			
		Q exp.	Q cal.	K_1 h^{-1}	R^2	Q_e exp.	Q_e cal.	K_1 h^{-1}	R^2

	10	11.007	2.152	0.3684	0.9409	11.007	11.088	0.700	0.9989
	20	9.128	1.677	0.4398	0.9669	9.128	9.192	1.008	0.9994
	30	9.021	1.669	0.4506	0.9729	9.021	9.112	0.981	0.9995
	50	8.814	1.590	0.4812	0.9673	8.814	8.903	1.084	0.9996

The findings displayed in Table 3 demonstrate that, for the pseudo-first order equation, Q_e (cal.) is larger than the experimentally determined Q_e (exp.), whereas, for the pseudo-second order equation, the calculated Q_e (cal.) values matched extremely well with the experimentally determined Q_e (exp.) values The R-squared value associated with the pseudo-second order kinetics exceeded those acquired from the pseudo-first order kinetics. It is evident that pseudo-second-order kinetics afforded a more accurate representation of the dye's adsorption on $CuFe_2O_4$ nanoparticles, suggesting that the adsorption system falls within this category. [35, 36].

Conclusions

$CuFe_2O_4$ nanoparticle ferrites were created in the current study utilizing the auto-combustion process of sol-gel. The single-stage spinel ferrite was achieved through the calcination of the material at 600 degrees Celsius. The impact of temperature, contact time, and pH among other factors, on the adsorption capacity were investigated. For CR dye, the contact duration was 360 minutes. It was discovered that the pseudo-second order kinetics rate expression well described the adsorption kinetics., while the equilibrium data exhibited a good fit with the Langmuir isotherm model with a maximum percentage removal of 77.83% occurring at pH=3. Thermodynamic analysis demonstrates the adsorption system's exothermic and spontaneous character. The produced chemical is thought to be a significant application for environmental preservation since it can be employed as a dye adsorbent.

References

[1] Zietz, B. P., Dieter, H. H., Lakomek, M., Schneider, H., Keßler-Gaedtke, B., & Dunkelberg, H. (2003). Epidemiological investigation on chronic copper toxicity to children exposed via the public drinking water supply. *Science of the Total Environment*, *302*(1-3), 127-144.

[2] Sokolowska-Gajda, J., Freeman, H. S., & Reife, A. (1996). Synthetic dyes based on environmental considerations. Part 2: Iron complexes formazan dyes. *Dyes and pigments*, *30*(1), 1-20.

[3] Gong, R., Li, M., Yang, C., Sun, Y., & Chen, J. (2005). Removal of cationic dyes from aqueous solution by adsorption on peanut hull. *Journal of Hazardous Materials*, *121*(1-3), 247-250.

[4] Young, L., & Yu, J. (1997). Ligninase-catalysed decolorization of synthetic dyes. *Water Research, 31*(5), 1187-1193.

[5] Puzyn, T., & Mostrag, A. (Eds.). (2012). *Organic pollutants ten years after the Stockholm convention: environmental and analytical update*. BoD–Books on Demand.

[6] Wang, S., Boyjoo, Y., & Choueib, A. (2005). A comparative study of dye removal using fly ash treated by different methods. *Chemosphere*, *60*(10), 1401-1407.

[7] Alshameri, A., Ibrahim, A., Assabri, A. M., Lei, X., Wang, H., & Yan, C. (2014). The investigation into the ammonium removal performance of Yemeni natural zeolite: Modification, ion exchange mechanism, and thermodynamics. *Powder Technology*, *258*, 20-31.

[8] Abood, M. I., & Jassim, T. E. (2018). Removal of methylene blue from aqueous solutions using Iraqi porcellanite rocks. *World J Pharm Res*, *7*(19), 230-243.

[9] Elsagh, A., Moradi, O., Fakhri, A., Najafi, F., Alizadeh, R., & Haddadi, V. (2017). Evaluation of the potential cationic dye removal using adsorption by graphene and

carbon nanotubes as adsorbents surfaces. *Arabian Journal of Chemistry*, *10*, S2862-S2869.

[10] Chamargore, J. J., Bharad, J. V., Madje, B. R., & Ubale, M. B. (2010). The removal of dye from aqueous solution by adsorption on low cost adsorbents. *Journal of Chemistry*, *7*, 1003-1007.

[11] Kefeni, K. K., Mamba, B. B., & Msagati, T. A. (2017). Application of spinel ferrite nanoparticles in water and wastewater treatment: a review. *Separation and Purification Technology*, *188*, 399-422.

[12] Tran, C. V., Quang, D. V., Nguyen Thi, H. P., Truong, T. N., & La, D. D. (2020). Effective removal of Pb (II) from aqueous media by a new design of Cu–Mg binary ferrite. *Acs Omega*, *5*(13), 7298-7306.

[13] Baig, R. N., & Varma, R. S. (2013). Magnetically retrievable catalysts for organic synthesis. *Chemical Communications*, *49*(8), 752-770.

[14] Baig, R. N., Nadagouda, M. N., & Varma, R. S. (2015). Magnetically retrievable catalysts for asymmetric synthesis. *Coordination Chemistry Reviews*, *287*, 137-156.

[15] Tran, C. V., Quang, D. V., Nguyen Thi, H. P., Truong, T. N., & La, D. D. (2020). Effective removal of Pb (II) from aqueous media by a new design of Cu–Mg binary ferrite. *Acs Omega*, *5*(13), 7298-7306.

[16] Prasad, S., & Gajbhiye, N. S. (1998). Magnetic studies of nanosized nickel ferrite particles synthesized by the citrate precursor technique. *Journal of Alloys and Compounds*, *265*(1-2), 87-92.

[17] Dehghanpour, H. R. (2016). Physical and chemical properties of NiFe 2 O 4 nanoparticles prepared by combustion and ultrasonic bath methods. *Russian Journal of Applied Chemistry*, *89*, 80-83.

[18] Shi, Y., Ding, J., Liu, X., & Wang, J. (1999). NiFe2O4 ultrafine particles prepared by co-precipitation/mechanical alloying. *Journal of Magnetism and Magnetic Materials*, *205*(2-3), 249-254.

[19] Salavati-Niasari, M., Davar, F., & Mahmoudi, T. (2009). A simple route to synthesize nanocrystalline nickel ferrite (NiFe2O4) in the presence of octanoic acid as a surfactant. *Polyhedron*, *28*(8), 1455-1458.

[20] Ismat, B., Nosheen, N., Munawar, I., Shagufta, K., Haq, N., Shazia, N., Yursa, S., Kashif, J., Misbah, S., Sadia, A., Fariha, R., & Mazhar, A. (2017). Green and eco-friendly synthesis of cobalt-oxide nanoparticle: Characterization and photo-catalytic activity. *Advanced Powder Technology*, *28*(9), 2035-2043.

[21] Hammood, A. Y., Mohammed, I. K., & Majeed, A. A. (2023). Removal of Cd(II) Ions from Aqueous Solutions using adsorption By Bentonite Clay and Study the Adsorption Thermodynamics. *Pollution,* 9(3), 994-1005.

[22] Ge, H., & Ma, Z. (2015). Microwave preparation of triethylenetetramine modified graphene oxide/chitosan composite for adsorption of Cr (VI). *Carbohydrate polymers*, *131*, 280-287.

[23] Anandan, B., & Rajendran, V. (2011). Morphological and size effects of NiO nanoparticles via solvothermal process and their optical properties. *Materials Science in Semiconductor Processing*, *14*(1), 43-47.

[24] Rajeh, A. A. H. (2018). The Effect of Catalyst Type on The Microstructure and Magnetic Properties of Synthesized Hard Cobalt Ferrite Nanoparticles. Journal of University of Babylon for Engineering Sciences, 26(4), 282-291.

[25] Cullity, B. D. (1956). *Elements of X-ray Diffraction*. Addison-Wesley Publishing.

[26] Hammood, A. Y., Jassim, T. E., & Al-Asadi, M. J. K. (2021), Use of nano-magnetic materials for removal of lead (II) & cadmium (II) ions from aqueous solutions, Mesopot. *Journal of Marine Science*, 36(1), 59 -72.

[27] El-Ashtoukhy, E. S., Amin, N. K., & Abdelwahab, O. (2008). Removal of lead (II) and copper (II) from aqueous solution using pomegranate peel as a new adsorbent. *Desalination*, *223*(1-3), 162-173.

[28] Pehlivan, E., Altun, T., & Parlayıcı, S. (2009). Utilization of barley straws as biosorbents for Cu2+ and Pb2+ ions. *Journal of hazardous materials*, *164*(2-3), 982-986.

[29] Bamroongwongdee, C., Suwannee, S., & Kongsomsaksiri, M. (2019). Adsorption of Congo red from aqueous solution by surfactant-modified rice husk: Kinetic, isotherm and thermodynamic analysis. *Songklanakarin Journal of Science & Technology*, *41*(5), 1076- 1083.

[30] Gilles, C. H., Macewan, T. H., Nakhwa, S. N., & Smith, D. (1960). A system of classification of solution adsorption isotherms, and its use in diagnosis of adsorption mechanisms and measurement of specific surface areas of solids. *Journal of the Chemical Society*, *2*, 3973-3993.

[31] Veena, M., & Robert, H. H. (2002). The Role of F-400 granular activated carbon in scavenging dissolved copper ions from aqueous solution. *Energeia*, *13*, 1-4.

[32] Elhussien, M. H., & Isa, Y. M. (2015). Acetic acid adsorption onto activated carbon derived from pods of acacia nilotica var astringens (sunt tree) by chemical activation with ZnCl2. *Journal of natural sciences research*, *5*(10), 42-48.

[33] Hefne, J. A., Mekhemer, W. K., Alandis, N. M., Aldayel, O. A., & Alajyan, T. (2008). Kinetic and thermodynamic study of the adsorption of Pb (II) from aqueous solution to the natural and treated bentonite. *International journal of physical sciences*, *3*(11), 281-288.

[34] Michot, L. J., & Villiéras, F. (2006). Chapter 12.9 Surface Area and Porosity. In F. Bergaya, B. K. G. Theng, & G. Lagaly (Eds.), *Developments in Clay Science* (Vol. 1, pp. 965-978). Elsevier.

[35] Abood, M. I., & Jassim, T. E. (2017). Adsorption equilibrium, kinetics and thermodynamics of Rhodamine B dye from aqueous solution using Iraqi Porcellanite rocks. *Mesopotamian Journal of Marine Sciences*, *32*(2), 88-103.

[36] Guillard, C., Puzenat, E., Lachheb, H., Houas, A., & Herrmann, J. M. (2005). Why inorganic salts decrease the TiO2 photocatalytic efficiency. *International Journal of Photoenergy*, *7*, 1-9.